Astron. Astrophys. 283, 729–744 (1994)

ASTRONOMY AND ASTROPHYSICS

A high-frequency radio continuum investigation of giant radio galaxies

I. Observations of six objects at 2.8 cm wavelength

U. Klein[1], K.-H. Mack[1,2], R. Strom[3], R. Wielebinski[2], and U. Achatz[2⋆]

[1] Radioastronomisches Institut, Universität Bonn, Auf dem Hügel 71, D-53121 Bonn, Germany
[2] Max-Planck-Institut für Radioastronomie, Auf dem Hügel 69, D-53121 Bonn, Germany
[3] Netherlands Foundation for Research in Astronomy, Sterrenwacht Dwingeloo, Postbus 2, NL-7900 AA Dwingeloo, The Netherlands

Received 24 June 1993 / Accepted 1 September 1993

Abstract. We have started a high-frequency radio continuum survey of giant radio galaxies (GRGs) with the aim to study the spectral index and polarization properties of these sources over a wide frequency range. Our measurements provide the necessary data base complementing low-frequency observations obtained with the WSRT. Here we report observations of NGC 315, DA 240, 4C 73.08, 3C 236, 3C 326, and NGC 6251 at λ2.8 cm, obtained with the Effelsberg 100-m telescope. Complete maps of the total and polarized emission of each source are presented, and their high-frequency radio morphologies as well as their magnetic field structures are discussed. While known jets and hot spots are detected, counter-jets are generally too weak and diffuse lobes are almost invariably narrower and more compact than at lower frequencies. The magnetic fields appear relaxed and remarkably uniform, as demonstrated by the high degrees of polarization (40%–60%) encountered. The outer edges of the hot spot regions are characterized by a circumferential magnetic field structure. This is probably the result of compression of the field caused by the ram pressure of the jets as they thrust through the intergalactic medium.

Key words: radio galaxies – linear polarization – magnetic fields

1. Introduction

The rare species of giant radio galaxies (GRGs) populates the extreme end of the linear size distribution of radio galaxies, with sizes in excess of 1 Mpc (H_0 = 75 km s^{-1} Mpc^{-1}). Although not representative, they allow the most detailed studies pertaining to the energy supply from the central engines and its relationship to their outer lobes. By their very nature they stretch models of double radio sources to the limit in certain realms of parameter space. Radio investigations of the extended components of GRGs have so far been restricted to relatively long wavelengths ($\lambda \lesssim 20$ cm), since single-dish measurements with adequate angular resolution have been rare, and observations with aperture synthesis techniques quickly become insensitive to the large-scale structure short of $\lambda \simeq 20$ cm. Systematic multi-frequency observations of GRGs with the WSRT were conducted by Willis & Strom (1978), Willis et al. (1978; 1981), Bridle et al. (1979), Strom & Willis (1980), Barthel et al. (1985), and Jägers (1986; 1987a,b). Measurements with the 100-m telescope at λ11 cm and 6 cm were reported by Stoffel & Wielebinski (1978) and by Strom et al. (1981), but a systematic high-frequency survey of GRGs and a full comparison with their low-frequency properties is still lacking. We therefore decided to fill this gap by employing the Effelsberg 100-m telescope at λ6.3 cm and 2.8 cm in order to completely map the largest radio galaxies, most of which have been observed with the WSRT at λ90, 49, and 21 cm.

Multi-frequency observations with similar angular resolution of GRGs are important for a number of reasons. The relativistic particles resident in their lobes have to cover much larger distances, thus bearing information about large fractions of the radio galaxies' lifetimes. Since they traverse large distances of intergalactic volume, they can also serve as diagnostic tools of the intergalactic medium (IGM) which is otherwise hardly accessible via direct observations. Therefore, the detailed study of their spectral behaviour as well as the magnetic fields that make them radiate will yield important information about the evolution of radio galaxies which in the case of GRGs must have taken place over a long period of time.

Measurements at short wavelengths are essential for two reasons: first, it is at the higher radio frequencies that particle aging is most pronounced, thus enabling studies of energy losses as a function of distance from the central source or hot spots. Closely related to this is the question whether in-situ acceleration out-

Send offprint requests to: U. Klein
⋆ Present address: Institut für Atmosphärenphysik, Schloßstr. 4-6, D-18225 Kühlungsborn, Germany

Table 1. Map parameters of GRGs

Source	Field centre		Final map size	Number of coverages			rms noise [mJy/b.a.]	
	α_{50} [h:m:s]	δ_{50} [°:′:″]	[′ × ′]	I	U	Q	I	σ_{Ip}
NGC 315	00:55:45.0	+30:00:00	60 ×43.3	12	11	11	1.7	0.6
DA 240	07:44:34.0	+55:56:47	36.7×30	11	11	11	1.3	0.6
4C 73.08	09:45:35.0	+73:29:33	23.3×16.7	8	8	8	0.9	0.5
3C 236	10:03:05.4	+35:48:08	70 ×70	10	9	8	1.2	0.5
3C 326	15:49:41.5	+20:13:49	30 ×16.7	7	7	7	1.2	0.8
NGC 6251	16:42:59.0	+82:28:21	70 ×70	12*	12*	12*	1.3*	0.5*

*see also Sect. 3.6

Table 2. Parameters of pointing and calibration sources

Source	α_{50} [h:m:s]	δ_{50} [°:′:″]	$S_{10.55GHz}$ [Jy]	$P_{10.55GHz}$ [%]	$\chi_{10.55GHz}$ [°]	
3C 48	01:34:49.83	+32:54:20.5	2.49	6.0	117	1,3
3C 123	04:33:55.20	+29:34:14.0	8.05	3.8	179	1,3
3C 138	05:18:17.53	+16:35:26.8	2.34	11.9	173	1,3
3C 286	13:29:49.66	+30:45:58.7	4.44	11.6	34	1,2,3
3C 295	14:09:33.50	+52:26:13.0	2.58	1.4	151	1,2,3
NGC 7027	21:05:09.40	+42:02:03.0	6.90	—	—	4

1: pointing; 2: total power calibration; 3: polarization calibration; 4: instrumental polarization

side the hot spots is necessary to explain the galaxies' radio morphology. Second, such observations are essentially free of Faraday effects and hence allow one to directly 'map' the intrinsic (projected) magnetic field structure as well as the degree of disorder and (de-) polarization characteristics if compared to low-frequency measurements.

Here we report observations of the GRGs NGC 315, DA 240, 4C 73.08, 3C 236, 3C 326, and NGC 6251 at λ2.8 cm, carried out with the 100-m telescope. On-going λ6.3 cm observations will be published later, and measurements of another sample of GRGs at these two wavelengths have commenced.

In Sect. 2 we describe the observations and data analysis, in Sect. 3 the maps of total intensity and linear polarization are presented, along with a brief description of their most salient properties as well as a first (qualitative) comparison with low-frequency maps, while the detailed comparisons will be presented in forthcoming papers. In Sect. 4 we finally discuss the results, and in Sect. 5 we summarize and draw first conclusions. Throughout this paper, we use $H_0 = 75\,\mathrm{km\,s^{-1}\,Mpc^{-1}}$.

2. Observations and data reduction

The measurements were made between August 1990 and February 1993 with the 10.6 GHz 4-horn, 8-channel receiver installed in the secondary focus of the 100-m telescope. The observational and data reduction procedure were the same as detailed by Gregorini et al. (1992). For each source, a field of size $(\theta_s + 23') \times (\theta_s + 2')$ where θ_s is the source extent in azimuth and elevation was scanned with a drive rate of 40′/min, and a scan interval of 20″. This field size definition accounts for the maximum beam throw involved in the multi-beam measurements. After restoration of the differential total-power maps to the equivalent single-beam maps (Emerson et al. 1979) these, as well as the single-beam Q and U maps, were combined to give final I, Q, and U maps in the azimuth–elevation frame. The large field sizes and observing times required a refinement of our program which interpolates such maps into a right ascension–declination coordinate system. Prior to this transformation the maps were subject to a routine which reduces baseline drifts by means of polynomial fits (Sofue & Reich 1979). The individual coverages have been averaged to yield final maps of Stokes parameters I, Q, and U. The Fourier filter technique of Emerson & Gräve (1988) was employed for those maps in which the variations of the parallactic angle across them were not too large.

We have at this stage not yet cleaned the maps as e.g. performed by Mack et al. (1993). Cleaning the large maps presented here is more difficult, owing to the rotation of the beam pattern across the field in right-ascension/declination. In the azimuth-elevation maps, on the other hand, the dirty beam suffers from serious distortion at large distances from the map centre. We are currently developing a CLEAN algorithm which works in the right-ascension/declination coordinate system. The cleaned maps will be presented and utilized in our subsequent analysis of the spectral index and polarization of the sources, to be published in forthcoming papers. Since the distortion introduced mainly affects emission near bright components, it has less consequences for the outer components mainly discussed here.

For further details concerning the telescope and receiver performance at 10.6 GHz we refer the reader to Gregorini et al. (1992).

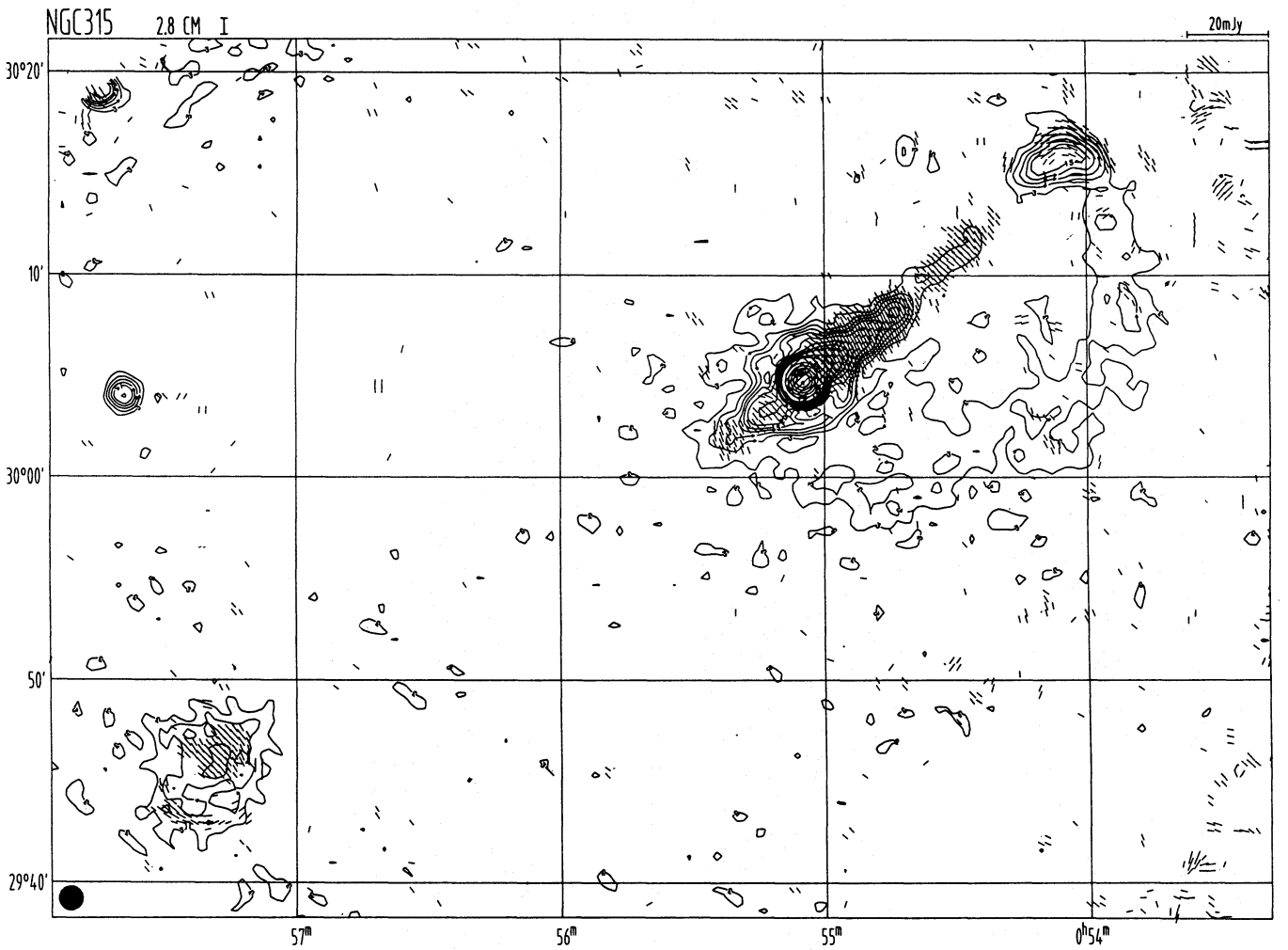

Fig. 1a. Map of the total intensity of NGC 315 at λ2.8 cm (see Table 4 for contour levels). Also shown are the **E**-vectors of the linearly polarized emission, but rotated by 90° to indicate the magnetic field orientation (see text). Their lengths are proportional to the polarized intensity, with the scale indicated by the small bar at the top right corner of the figure. The hatched circle in the lower left indicates the 3 dB beam size

Table 3. Source parameters of the GRGs

Source	z	D^* [Mpc]	s.c.r.†
NGC 315	0.0167	66	0.341
DA 240	0.0356	137	0.665
4C 73.08	0.0581	220	1.065
3C 236	0.0988	360	1.743
3C 326	0.0895	329	1.593
NGC 6251	0.0234	91	0.444

* $H_0 = 75\,\mathrm{km\,s^{-1}\,Mpc^{-1}}$; $q_0 = 1$
† size conversion ratio: kpc/arcsec

Table 1 summarizes the relevant map parameters of each source. The final field sizes given here refer to a region of largely uniform noise: owing to our azimuth–elevation maps the coverage by individual measurements decreases towards the edges of the beam-centred right ascension–declination maps, resulting in an increase of noise towards their edges. In Table 2 we list the sources used for calibration and pointing, along with their position, flux densities, and polarization parameters. The flux density scale is that of Baars et al. (1977).

3. Results and discussion

In what follows we shall present the λ2.8 cm maps of the GRGs. Some parameters relevant to the objects are given in Table 3, the contour levels of the maps have been compiled in Table 4. We discuss the results of each source individually. A more detailed interpretation will be presented in Sect. 4.

3.1. NGC 315

The z-shaped large-scale morphology of this GRG was first noted by Bridle et al. (1976) who mapped it at 0.43, 1.41, and 2.38 GHz using the Arecibo 300-m telescope. Stoffel & Wielebinski (1978) published a 2.7 GHz map obtained with the Effelsberg 100-m dish, which shows strong linear polarization over most of the source, reaching 46% in the bridge towards

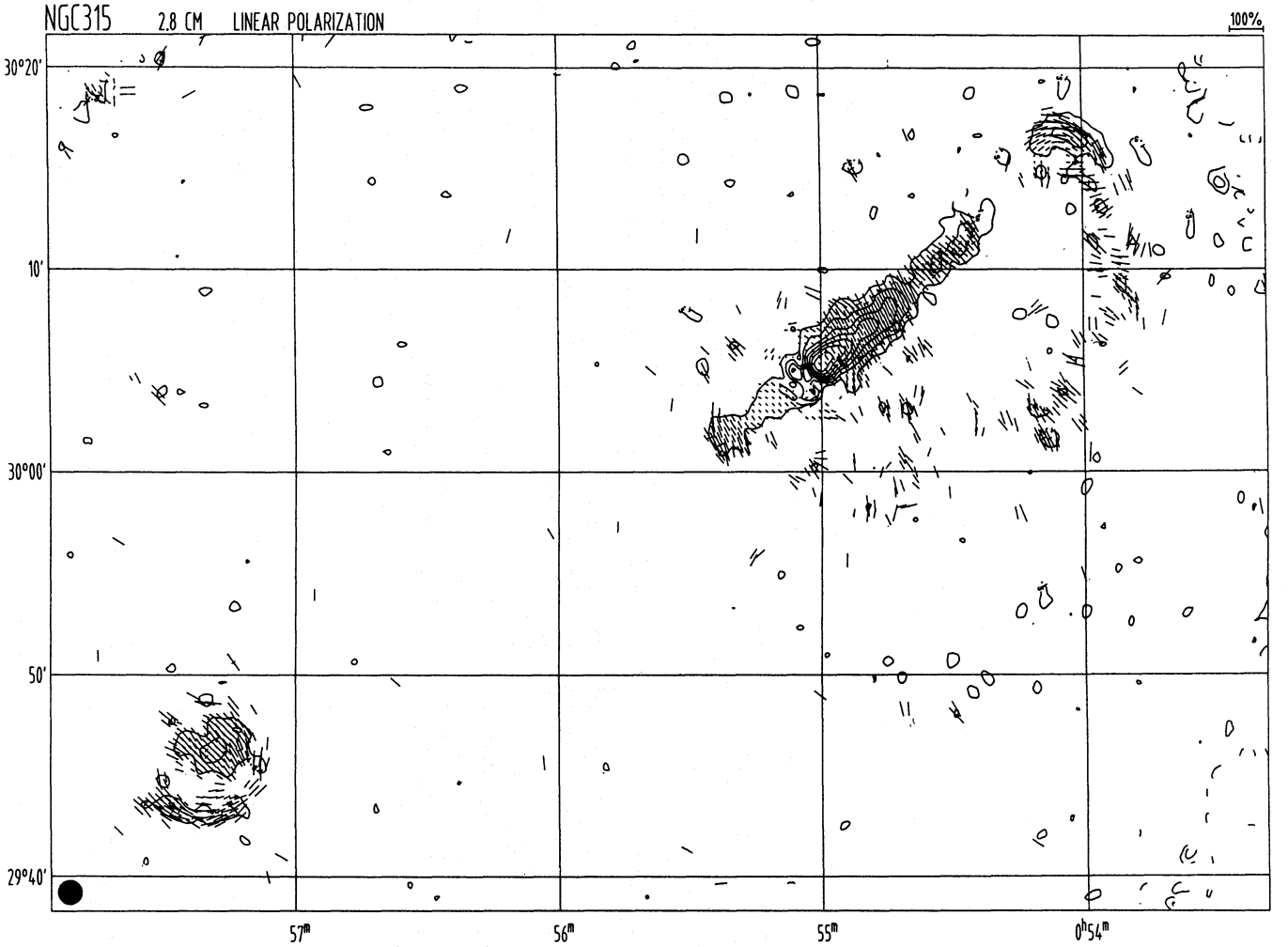

Fig. 1b. Map of the linearly polarized intensity of NGC 315 at λ2.8 cm. The **E**-vectors, again rotated by 90°, have lengths proportional to the fractional polarization. Their scale is indicated by the bar at the top right of the figure

Table 4. Contour levels of the maps

Source	Fig.	Contour levels
NGC 315	1a	3,6,...,15,20,30,...,50,75,100,200,...,700 mJy/b.a.
	1b	1.5,3,...,9 mJy/b.a.
DA 240	2a	3,6,...,15,19,24,30,40,50,75,100,150,...,250 mJy/b.a.
	2b	1.25,2.5,6,9,...,15,20,30,...,50 mJy/b.a.
4C 73.08	3a	3,6,...,30,36,...,72 mJy/b.a.
	3b	1.25,2.5,4,6,...,14 mJy/b.a.
3C 236	4a	3,6,...,15,20,...,40,60,...,100,150,...,800 mJy/b.a.
	4b	1.5,3,5,7,10 mJy/b.a.
3C 326	5a	2.5,5,...,10,13,25,30,...,45 ,Jy/b.a.
	5b	1.5,3,...,9 mJy/b.a.
NGC 6251	6a	3,6,...,15,20,30,40,60,80,100,150,200,300,...,600 mJy/b.a.
	6b	1,2,3,5,7,9,12 mJy/b.a.

the north-western lobe at this angular resolution (4.″4). The first high-resolution interferometric observations were made by Bridle et al. (1979) at 610 MHz with the WSRT and at 1465 and 4885 MHz with the VLA, revealing narrow jets which connect the central compact source to the outer lobes. The first systematic investigation of the spectral index and polarization properties of the jets and lobes of NGC 315 was conducted by Willis et al. (1981), who used the WSRT at λ49 cm and λ21 cm, followed by improved observations with the upgraded WSRT by Jägers (1986; 1987a).

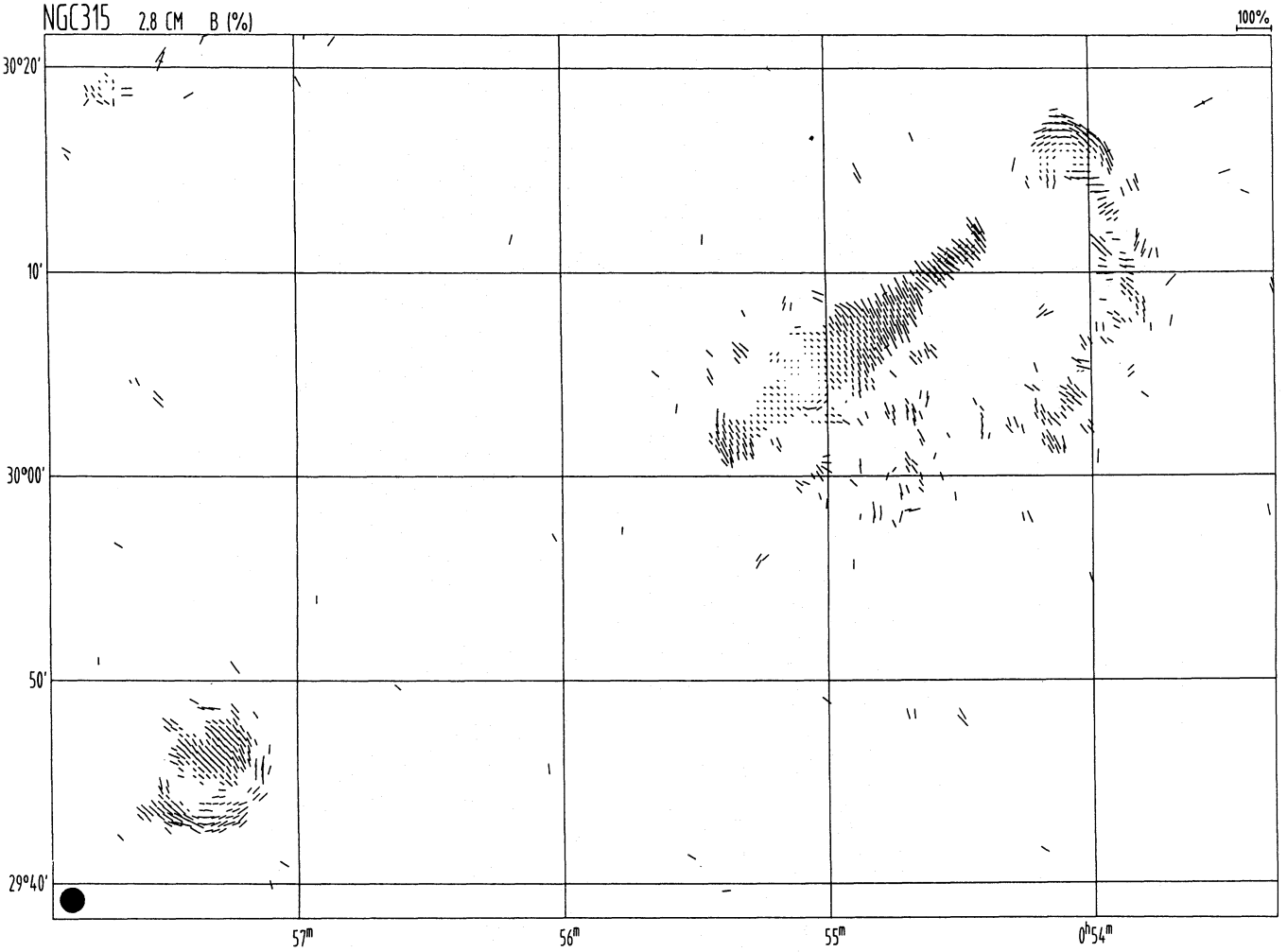

Fig. 1c. Projected magnetic field orientation in NGC 315. The vectors shown here are identical to those superimposed in Fig. 1b

Our λ2.8 cm map is shown in Fig. 1a, superimposed by $\boldsymbol{B}$-vectors, with their lengths proportional to the polarized brightnesses. These $\boldsymbol{B}$-vectors have been obtained by just rotating the $\boldsymbol{E}$-vectors by 90°, assuming negligible Faraday rotation at λ2.8 cm. The bright central core, which has an inverted spectrum (Fanti et al. 1976), has a flux density of $\sim$ 720 mJy at this wavelength. This source produces appreciable spurious effects in its immediate vicinity, which is the effect of combining the beam pattern at various parallactic angles. The prominent jet/counterjet system is well visible in Fig. 1a. The counterjet can be traced out to a distance of $\sim$ 5'.8 (120 kpc). This closely corresponds to the distance at which the north-western jet undergoes a sudden decrease in brightness. This was already visible, though less pronounced, in the λ21 cm map of Willis et al. (1981) and noted by these authors. No emission is seen above the noise level of this map between the termination of the counterjet and the extended south-eastern lobe, while the north-western jet can be traced almost out to the lobe. This lobe has embedded a double hot spot from which a prominent 'loop' of low-level emission bends back southward and fades away south of the core of NGC 315. The faint emission extending northwards from the south-eastern lobe which is visible at lower frequencies (cf. the maps of Stoffel & Wielebinski 1978; Willis et al. 1981 and Jägers 1987) has disappeared at 10.6 GHz.

In Fig. 1b we present the map of linear polarization of NGC 315 at λ2.8 cm. Comparing with the λ49 cm and 21 cm maps of Willis et al. (1981) and Jägers (1987), there is surprisingly little change in the distribution of polarized emission over a wide frequency range, implying little depolarization at lower frequencies. Again, $\boldsymbol{B}$-vectors are superimposed, their lengths being proportional to the degree of polarization. For the sake of clarity we display these $\boldsymbol{B}$-vectors once more in Fig. 1c. Both jets are characterized by a perpendicular $\boldsymbol{B}$-field. In the north-western lobe the field is initially perpendicular to the jet axis, but then appears to be aligned along the outer lobe edge, swinging around as the hot spots merge into the faint loop. In the loop it is largely perpendicular again, but cannot be traced continuously because of the patchy distribution of the fractional polarization. The counterjet, too, features a perpendicular field. In the centre of the south-eastern lobe the magnetic field is oriented perpendicular to the jet axis, but a circumferential component appears to embrace most of the outer lobe structure. It thus appears as if

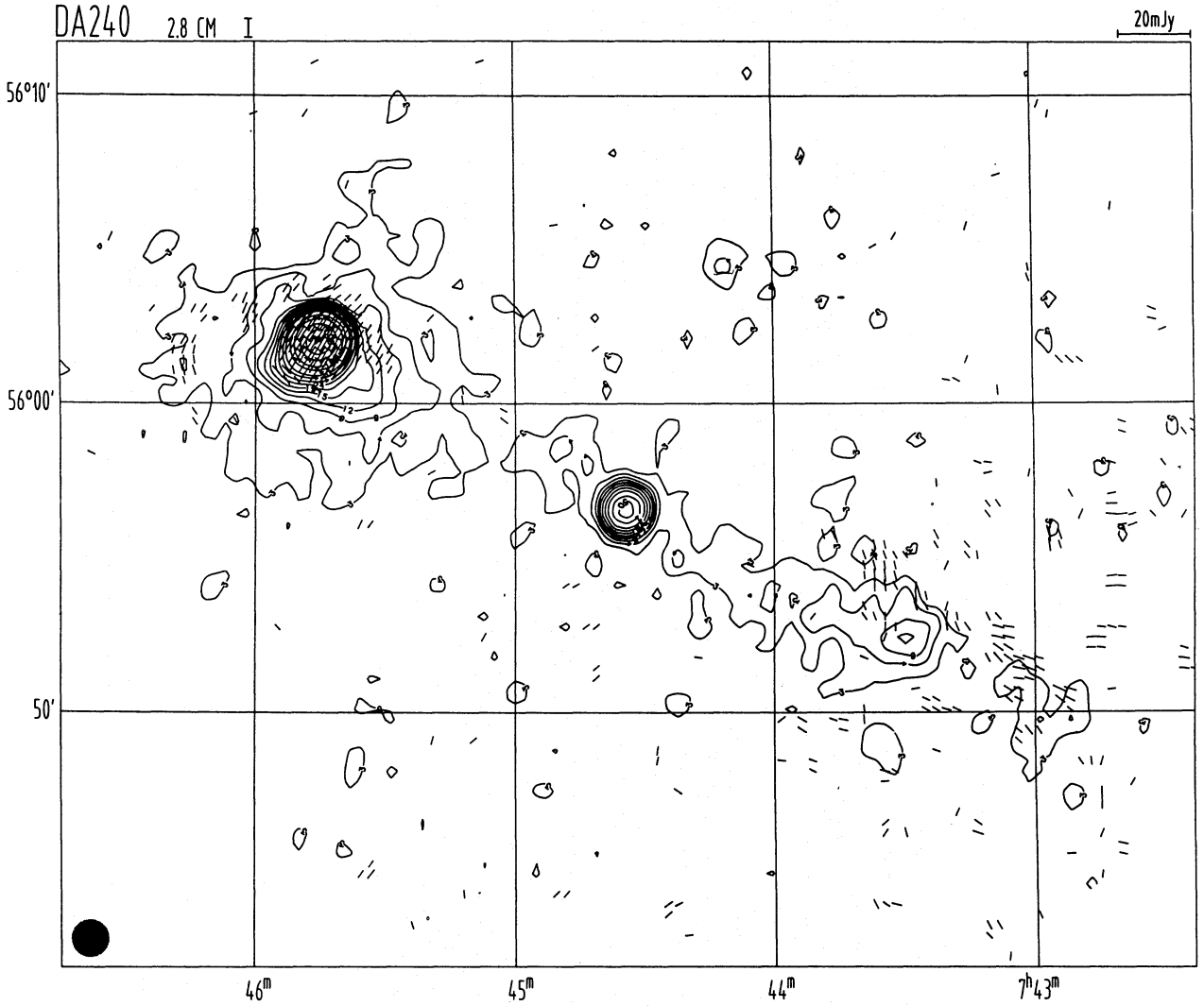

Fig. 2a. Map of the total intensity of DA 240 at λ2.8 cm (same layout as in Fig. 1a)

the projected magnetic field structure reflects its compression at the outer source periphery as the jet material is impinging on the intergalactic medium (IGM) and comes to a halt. It is noteworthy that the magnetic field mapped here resembles that derived by Willis et al. (1981) very closely, except in a few locations (see Fig. 1c).

The highest degrees of linear polarization at λ2.8 cm are found within the faint part of the main jet, and at the outer edges of the lobes, with maximum values of $p_{2.8} \approx 50\%$. These are close to the theoretical maxima and imply an almost perfect ordering of the magnetic field at these locations. This is not surprising along the edge of a component, where the short path length will minimize the effects of superposition of fields with different orientations. Strong polarization ($\sim$ 30%) is found over most of the source except close to the nucleus, where it drops to the instrumental response ($\lesssim$ 1%). This is probably the result of the transition of the magnetic field (Fomalont et al. 1980) from running parallel to the jet to perpendicular (field components perpendicular to each other yield zero net polarization). Surprisingly, fairly high degrees of linear polarization are also found in some locations of the giant loop swinging back south of the galaxy, with values of $p \sim 30$–40% indicating good field alignment in this presumably aged component! One may speculate at this point that this field ordering may support the containment of relativistic particles while they suffer synchrotron and inverse Compton losses. Note that this 'old lobe' is visible between 327 MHz (Willis & O'Dea 1990) and 10.6 GHz! This is not the case in the low-brightness northern continuation of the south-eastern lobe, which is only seen at frequencies $\lesssim$ 5 GHz.

3.2. DA 240

This GRG was first studied in detail at λ49 cm by Willis et al. (1974) and at λ11 cm by Baker et al. (1974). It is characterized by its two nearly circular lobes (see Strom et al. 1981) and could thus be ranked as a 'fat double' (Muxlow & Garrington 1991). However, in contrast to other objects in this species, DA 240

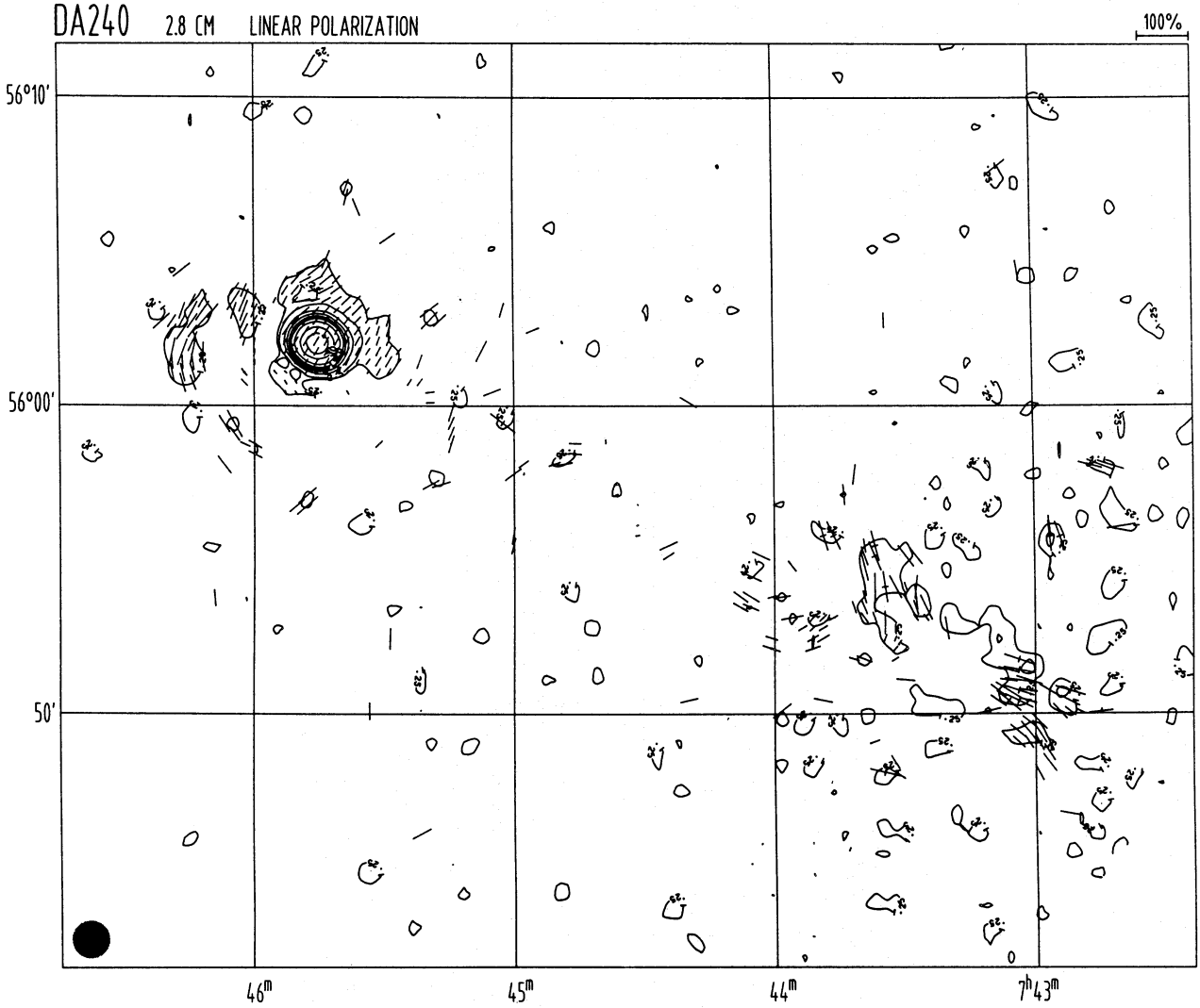

Fig. 2b. Map of the linearly polarized intensity of DA 240 at λ2.8 cm (same layout as in Fig. 1b)

exhibits ongoing central activity and is therefore not a fully relaxed source.

Our λ2.8 cm map (Fig. 2a) shows a considerable brightness asymmetry of DA 240: the brightest source is 4C 56.16, the hot spot in the eastern lobe, while the western hot spot is much less pronounced at this wavelength. The central source is more pronounced than at low frequencies, with a peak brightness of 57 mJy/b.a. This overall high-frequency behaviour thus confirms the spectral index trends derived by Strom et al. (1981) and Tsien (1982). Figure 2a indicates a considerable steepening of the radio spectrum in the extended lobes, especially in the western one, which at λ2.8 cm has entirely lost its circular shape visible at low frequencies. The lobes are connected to the central source by a low-brightness bridge of emission, which is also seen at lower frequencies (Strom et al. 1981; Stoffel 1978). Note, however, that at higher resolution the lobes appear distinct from the core (Jägers 1987b).

The distribution of linear polarization at λ2.8 cm, shown in Fig. 2b, is substantially different from that seen e.g. in NGC 315. The bridge of emission connecting the core to the outer lobes is largely unpolarized. The strongest polarization is seen at the eastern hot spot, with degrees of polarization of $p_{2.8} \simeq$ 20-50%, i.e. they are far above the instrumental response. The polarized brightness in the western lobe is low, but its fractional polarization is high, with average values of $p_{2.8} \simeq 50\%$. This clearly confirms the trends reported by Baker et al. (1974) and Tsien (1982). There is also a clear difference in the magnetic field orientation between the eastern and western lobe. In the latter, it is predominantly parallel to the faint outer elongated feature preceding it ($\alpha_{50} = 7^h43^m$, $\delta_{50} = 55°50'$), and it shows a complex structure in the central part of this lobe. This is corroborated by the low polarization at $\alpha_{50} = 7^h43^m30^s$, $\delta_{50} = 55°52'25''$, which is certainly the result of beam depolarization, given the small rotation measures evaluated by Tsien (1982). In the eastern lobe the field is perpendicular within and around the hot spot, and circumferential in the lobe's outskirts as far as it has been detected. Our observations thus confirm the magnetic field mor-

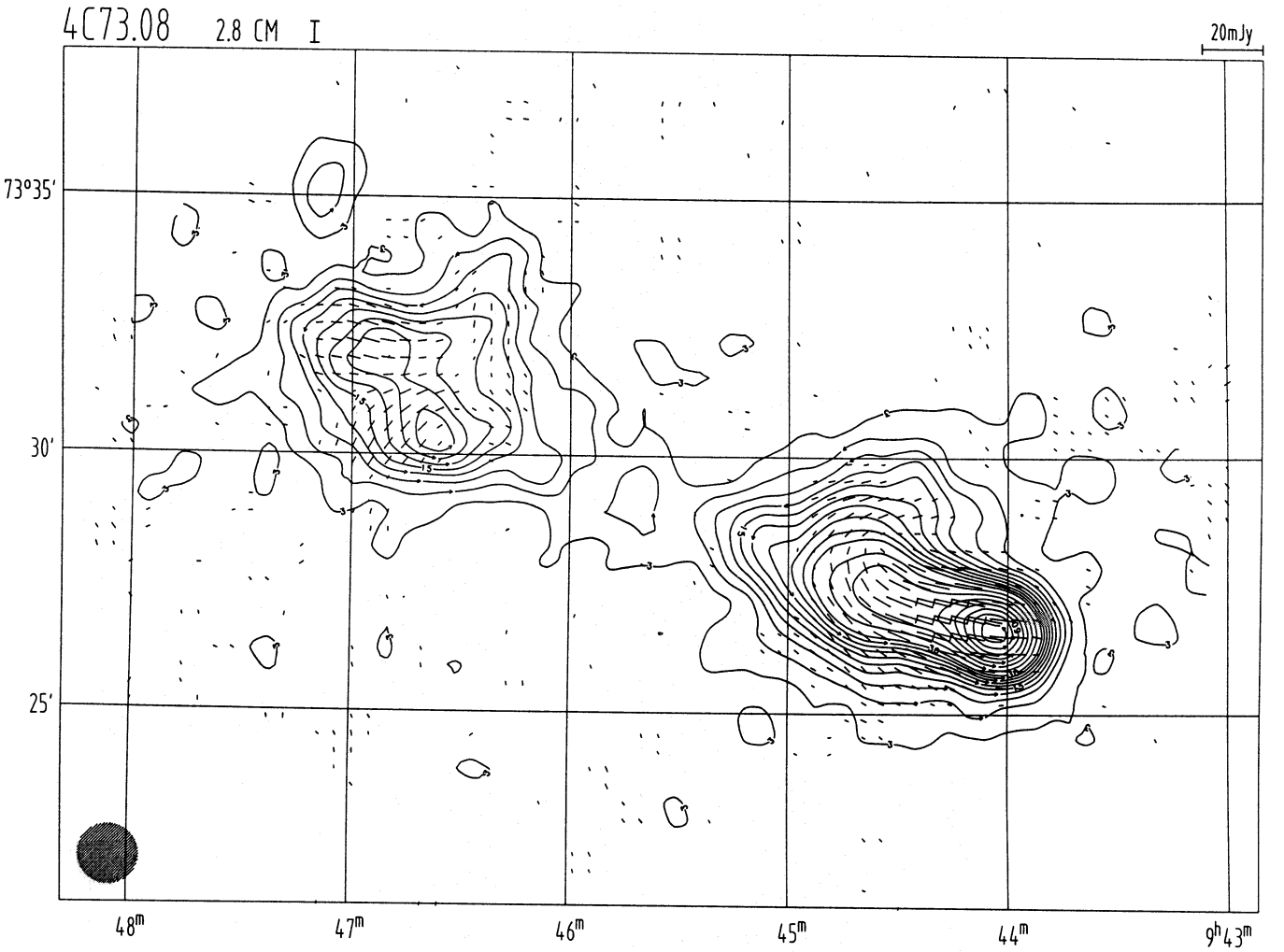

Fig. 3a. Map of the total intensity of 4C 72.08 at λ2.8 cm (same layout as in Fig. 1a)

phology discussed by Tsien (1982), who had to assume small values of Faraday rotation.

It is tempting to apply the compression model of Laing (1980) to the circumferential magnetic field around the eastern lobe, but the question remains what makes the B-field structure in the western one so different. By the same token, the swing of the magnetic field in the north-western lobe of NGC 315 and the circumferential field at the outer edge of its south-eastern one could be caused by this very mechanism.

3.3. 4C 73.08

The first radio continuum investigation of this GRG was made by Mayer (1979). Jägers (1986) made a multi-frequency study at 327, 609, and 1412 MHz using the WSRT. The peculiar source morphology of 4C 73.08 may to some extent result from precession of the central object, but one probably has to invoke motion through and interaction with the surrounding IGM (Jägers 1986).

These peculiar source structures, in particular the protrusions out of each lobe due north (denoted L_1 and L_1' by Jägers), are also salient features in our λ2.8 cm map, which is shown in Fig. 3a. Protrusions L_2 and L_2' (Jägers 1986), which emerge to the south of each lobe, are much less conspicuous at this wavelength. Compared with the low-frequency maps of Jägers (e.g. his 327 MHz map), the λ2.8 cm emission confirms the spectral index trends that he derived. In particular, the hot spot in the western lobe is the brightest region in the map. The lobes are connected by a low-level bridge of emission, with a small maximum ($\sim$ 4 mJy/b.a.) located at $\alpha_{50} \simeq 4^{\rm h}45^{\rm m}41\overset{\rm s}{.}4$, $\delta_{50} \simeq 73°29'10''$. This peak is not coincident with any of the sources visible at lower frequencies and at higher resolution. Its nearly perfect position on the source major axis and half-way between the lobes may be accidental.

As at lower frequencies, the linear polarization (Fig. 3b) exhibits a complex structure, which largely even resembles that seen at 327 MHz with about the same angular resolution. This hints at very low rotation measures. Strong polarization is measured over most of the source, with the highest values ($p_{2.8} \simeq 50$–60%) occurring at the ends of the southern and northern protrusions of the lobes. Lower degrees of polarization are likely due to beam depolarization, which results

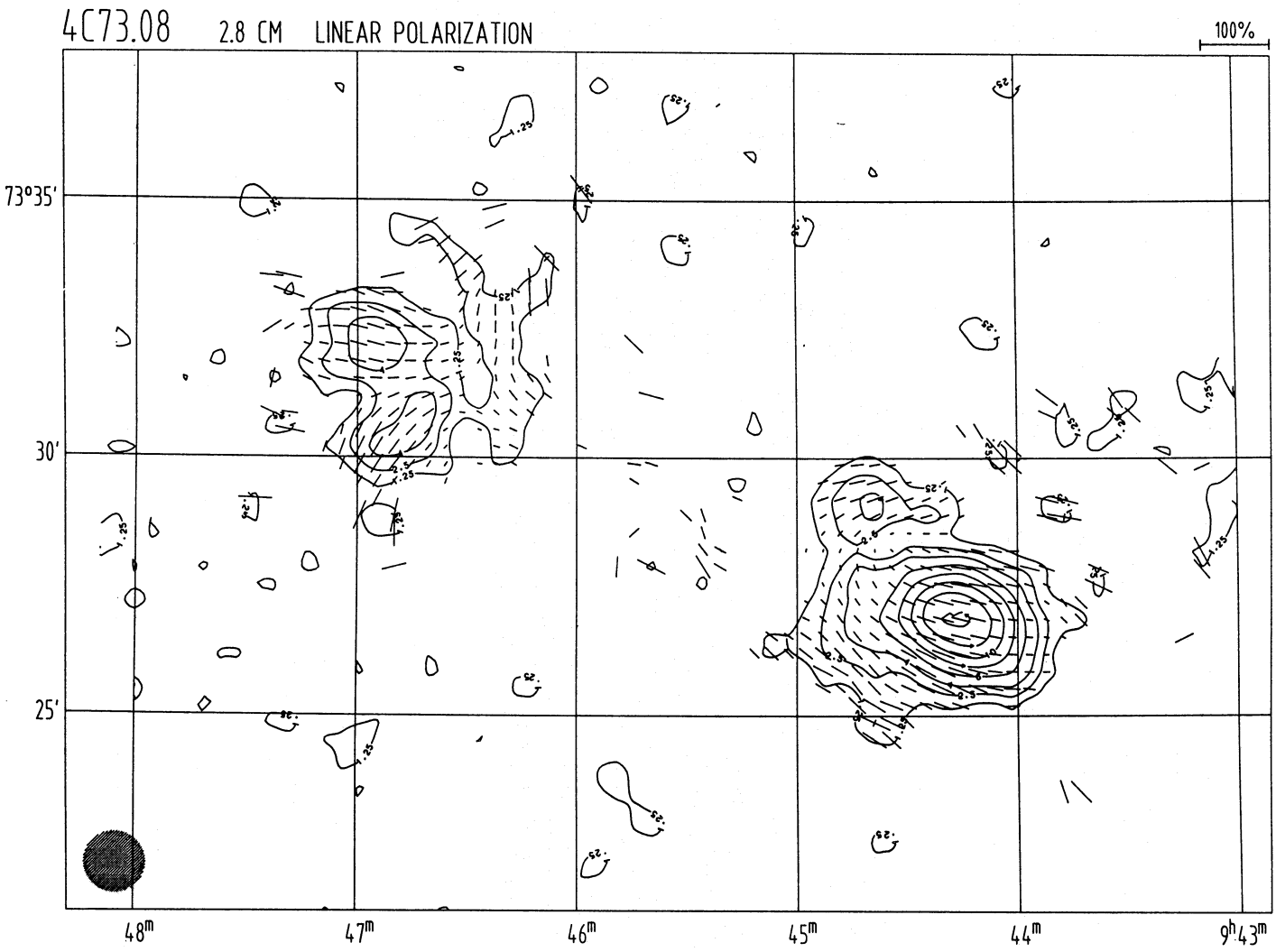

Fig. 3b. Map of the linearly polarized intensity of 4C 73.08 at λ2.8 cm (same layout as in Fig. 1b)

from the (presumably highly aligned) magnetic field swinging around. Strong bends of the magnetic field are in fact seen at the commencements of the protrusions, and it appears that the field follows precisely these anomalous emission features (compare Fig. 3b and the λ21 cm map of Jägers 1986). Jägers has determined the magnetic field morphology on the basis of his 3-frequency measurements. However, our observations do not confirm his results.

3.4. 3C 236

This largest known radio source was first recognized as a huge radio galaxy by Willis et al. (1974) based on high-resolution observations at λ49 cm. That work was followed by a thorough investigation of its structure, spectral index, depolarization, rotation measure, and magnetic field by incorporating measurements at $\lambda\lambda$49, 21, and 6 cm (Strom & Willis 1980). The relation of the small- and large-scale structure of 3C 236 was discussed by Barthel et al. (1985). Willis & O'Dea (1990) published a λ90 cm map. This largest known radio source has seen very comprehensive low-frequency studies.

Our λ2.8 cm map, shown in Fig. 4a, is at this stage less sensitive than the other maps presented here, owing to less integration time. Figure 4a shows the bright central source as well as the north-western and south-eastern lobes. The bridge seen at lower frequencies and connecting these components is not (yet) seen at the current noise level, supporting the steepening of the spectrum inwards from the lobes reported by Strom et al. (1981). As in the case of NGC 315, the beam pattern is seen to surround the central source, which will be CLEANed at a later stage. The flux density of this nuclear source at λ2.8 cm is 900 mJy. As at lower frequencies (Strom & Willis 1980) the preceding lobe (1002+35) is essentially resolved, while the structure of 1004+34 is dominated by two bright sources. The north-western one, which corresponds to source E as denoted by Strom & Willis, is a background source (ibidem, see also Willis et al. 1974). The eastern one, forming the termination of the lobe, is the hot spot of this lobe. The steep spectrum source E seen at $\alpha_{50} = 10^h04^m47^s$, $\delta_{50} = 34°53'29''$, is barely visible at λ2.8 cm.

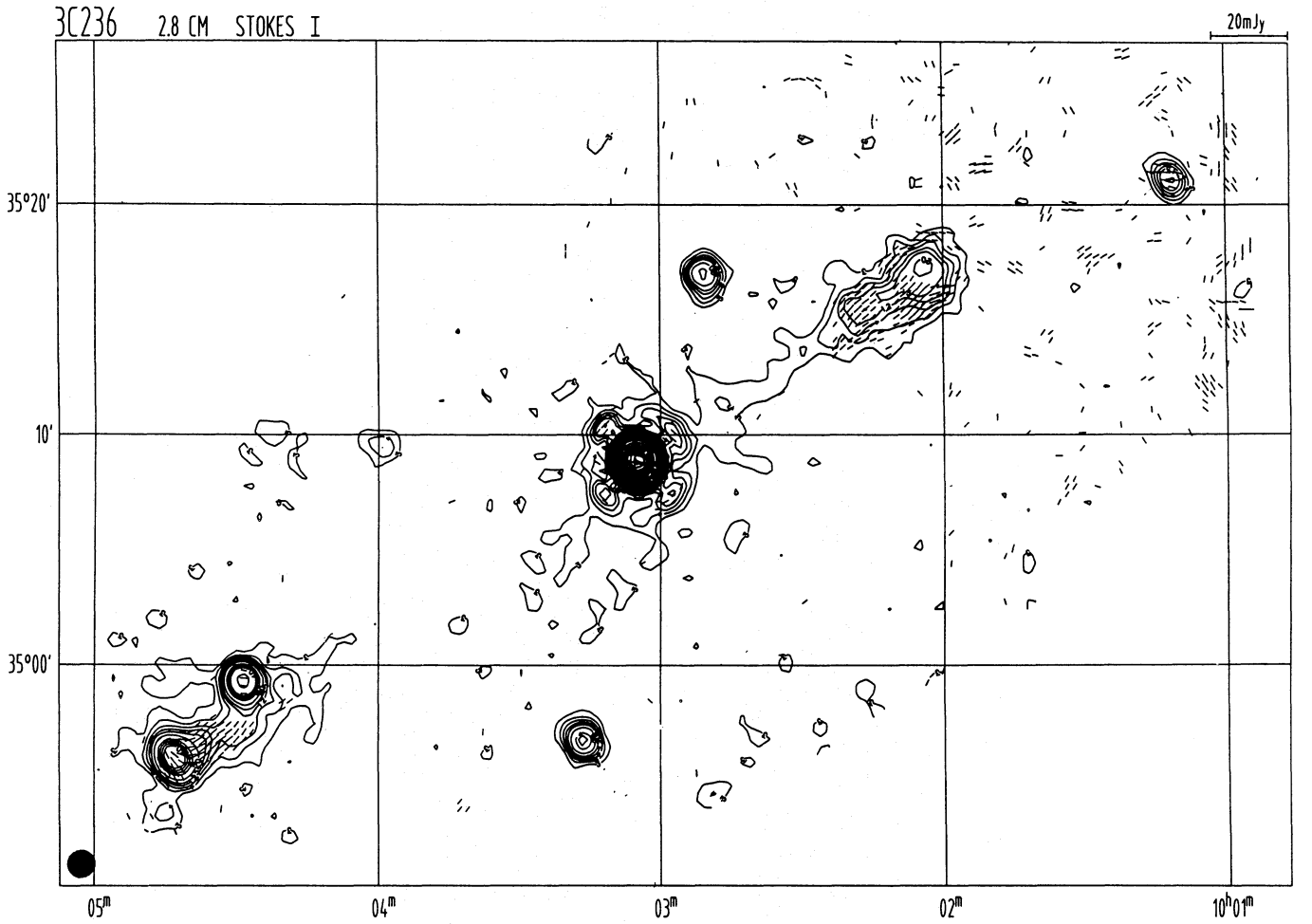

Fig. 4a. Map of the total intensity of 3C 236 at λ2.8 cm (same layout as in Fig. 1a)

Extrapolating its low-frequency spectrum, we would expect some 10 mJy at this wavelength, while the measured flux density is $\lesssim$ 4 mJy, implying that the spectrum steepens further. This further corroborates that it is a background source, unrelated to 3C 236. The source at $\alpha_{50} = 10^h01^m11^s.4$, $\delta_{50} = 35°21'02''$ is probably unrelated to 3C 236, as it is off-axis from the otherwise perfectly linear structure of the radio galaxy. Furthermore, the magnetic field appears to confine the lobe at $\alpha_{50} \approx 10^h02^m$ (see Fig. 4b), which is a frequent finding in the sources studied here.

In Fig. 4b our map of linear polarization of 3C 236 at λ2.8 cm is shown. The outer lobes do show up as strongly polarized regions, with maximum degrees of $\sim$ 30–40%. The nuclear source produces a purely instrumental response. The lobes exhibit a magnetic field parallel to the source axis, which becomes circumferential at their terminations. In 1002+35 the degree of polarization is drastically lower along the ridge line, and rises rapidly towards the lobe's outer edges, a trend that was already noticed by Strom & Willis (1980). In 1004+34 the hot spot shows lower degrees of polarization ($\sim$ 10%), except at its outer edge. This probably results from beam depolarization as the magnetic field swings around from parallel to the source axis to perpendicular. On the whole, the magnetic field observed here closely resembles that deduced by Strom & Willis (1980) on the basis of a rotation measure analysis.

3.5. 3C 326

The structure of this GRG was first studied by Mackay (1969) who used the Cambridge One Mile Telescope at 408 and 1407 MHz. This study was followed by single-dish observations by Bridle et al. (1972) and Baker (1974), and the latter author was the first to hint at the large intrinsic size of this radio source. A thorough multi-frequency investigation of 3C 326 was carried out by Willis & Strom (1978) who used the WSRT at $\lambda\lambda$49, 21, and 6 cm. They studied the distribution of the spectral index, the rotation measure and depolarization, as well as the magnetic field structure across this source. Their measurements disclosed the existence of a well-ordered magnetic field over large scales, up to $\sim$ 550 kpc.

Our λ2.8 cm map is displayed in Fig. 5a. Comparison with the 327 MHz map of Willis & O'Dea (1990) and that at 610 MHz of Willis & Strom (1978) shows that all low-frequency components are also detected at 10.6 GHz. The nuclear source ($\alpha_{50} = 15^h49^m56^s.1$, $\delta_{50} = 20°14'17''$) has a flux density of

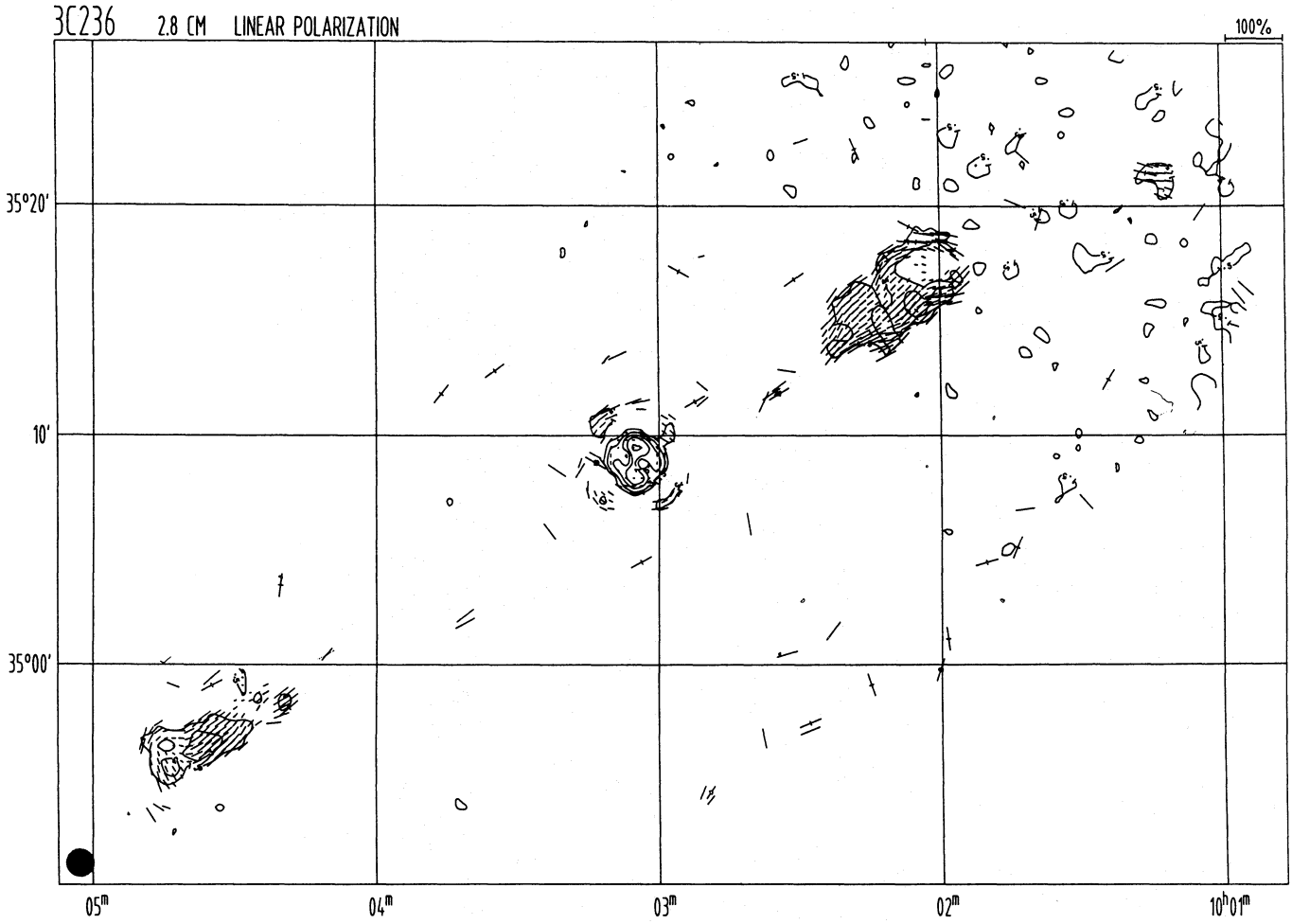

Fig. 4b. Map of the linearly polarized intensity of 3C 236 at λ2.8 cm (same layout as in Fig. 1b)

$\sim$ 10 mJy at 10.6 GHz, implying a spectral index of $\alpha = -0.31$ ($S_\nu \sim \nu^\alpha$), which is somewhat steeper than at lower frequencies (Willis & Strom 1978). The two lobes look rather different at this wavelength (see Fig. 5a). The western one forms a linear structure which widens towards the central source although it seems noticeably narrower than at the lower frequencies. It has its maximum brightness at the location of the presumed two hot spots (Willis & Strom 1978) located at its western edge. These have been convolved into a bright elongated source by our 69″ beam. In contrast, the eastern lobe is shorter and broader, with extensions to the south-east and east. The two bright background sources seen by Willis & Strom (1978) are also still visible at λ2.8 cm.

Figure 5b shows the map of linear polarization of 3C 326 at λ2.8 cm. Strong polarization is found in the western lobe, with degrees in excess of 60%. This is in line with the coherent magnetic field structure evident in this map. At the location of the lobe's flaring towards the central sources the polarization drops abruptly to values $<$ 15%, certainly the result of beam depolarization by the more complex magnetic field in this region where it appears to flare up, similar to the total power emission (see also Fig. 5a). The outer edge of the western lobe shows lower degrees of polarization, $p_{2.8} < 20\%$. The eastern lobe is less polarized, with $p_{2.8} \simeq 8\%$. Higher values ($\sim$ 30%) are only found at its southern edge, in accord with the findings of Willis & Strom. In the south-eastern part of this lobe, the degrees of linear polarization fall below $\sim$ 8%, indicating a tangled field structure there. On the whole, the magnetic field in the eastern lobe is along the source axis of 3C 326. There is no indication for the magnetic field to be circumferential to the lobe or perpendicular to the source axis at the lobes' terminations as is seen in most of the other sources studied here.

3.6. NGC 6251

Waggett et al. (1977) were the first to investigate this large radio source and to rank it among the GRG class, based on their measurements at 151 and 1407 MHz. They also discovered the 200 kpc long jet emerging on the north-western side of the nucleus and reaching into the complex north-preceding lobe. Subsequently, maps of NGC 6251 were made by Willis et al. (1978) and by Jägers (1987) with the WSRT at 610 MHz and by Stoffel & Wielebinski (1978) with the Effelsberg 100-m telescope at 2700 MHz. These also contained the distribution of linear po-

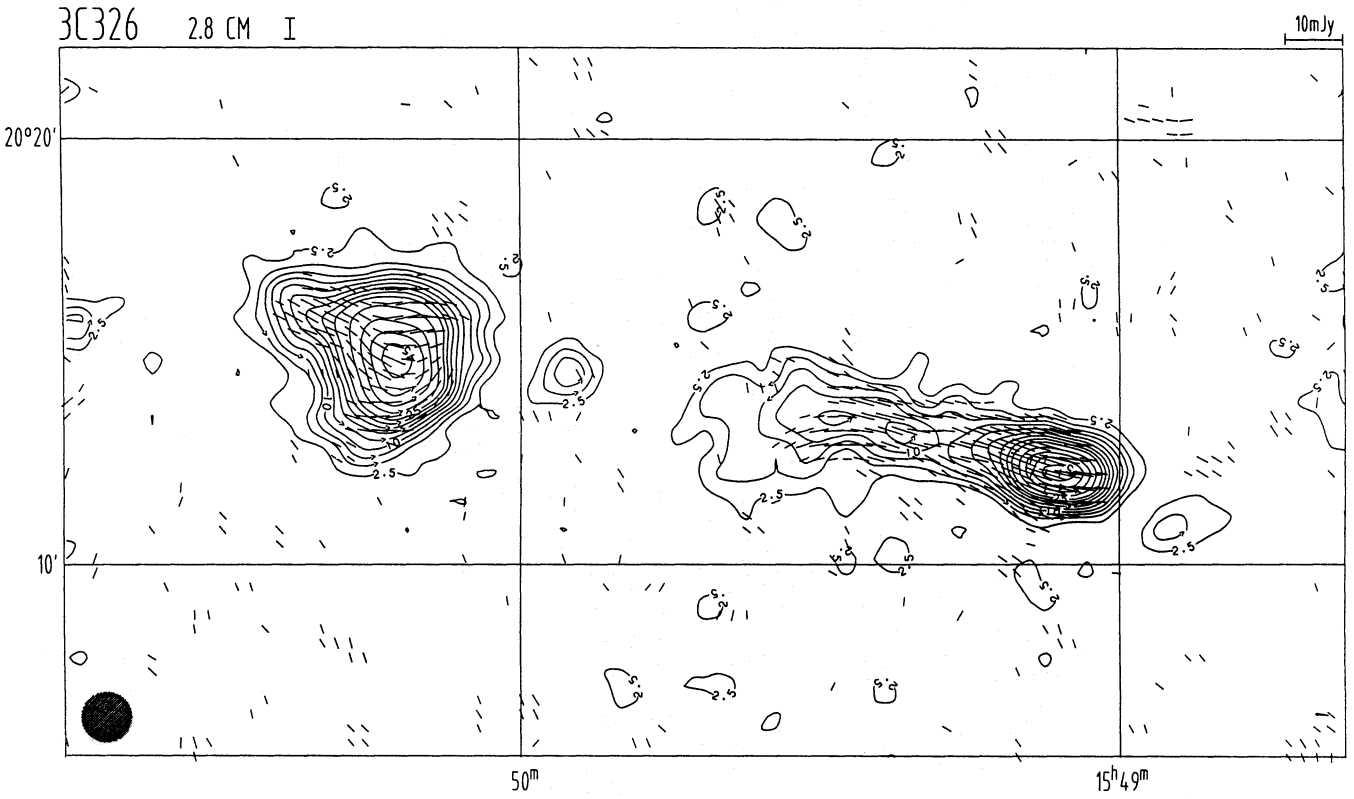

Fig. 5a. Map of the total intensity of 3C 326 at λ2.8 cm (same layout as in Fig. 1a)

larization across this source, and uncovered high degrees (up to 70% at 610 MHz) of polarization in the north-western lobe. An improved WSRT map at 610 MHz as well as a first study of the polarization of the prominent jet with the VLA at 1662 MHz was presented by Willis et al. (1982). This jet was investigated in great detail by Saunders et al. (1981) and by Perley et al. (1984).

Our λ2.8 cm map of NGC 6251 is shown in Fig. 6a. The noise in the region centred on α_{50} = $16^h34^m41^s.3$, δ_{50} = 82°42′39″ has been improved by a weighted addition of another 7 coverages of $\sim$ 22′ × 22′ extent. The influence on the level of the polarization map (due to its Ricean noise distribution, see Wardle & Kronberg 1974) is only marginal ($\sim$ 0.05 mJy/b.a.). The noise levels in this area are σ_I = 0.7 mJy/b.a., σ_{Ip} = 0.3 mJy/b.a. The central source has a flux density of 810 mJy at λ2.8 cm. The jet is clearly depicted in Fig. 6a, with a pronounced brightening at $\sim$ 3′.6 from the nucleus, which is also seen at lower frequencies. Much of the plateau-like structure surrounding the central source and the inner bright jet is due to the sidelobe pattern. Cleaning is mandatory here, too.

The extent of the large north-western lobe has shrunk dramatically at this wavelength, indicating a strong steepening of its radio spectrum (comp. Fig. 1 of Willis et al. 1982). This is readily evidenced by the source at $\alpha_{50} \approx 16^h31^m$, δ_{50} = 82°42′, which was suspected to belong to the lobe complex by Willis et al. (1978) because of the extended emission which it is embedded in at lower frequencies. However, the lack of linear polarization of this source at λ2.8 cm (also noted by Willis et al.) leads us to conclude that it is a background source after all, since almost all of the radio source components of the source studied here are characterized by appreciable amounts of polarization. The steepening of the spectrum in this area was also indicated in the investigations by Waggett et al. (1977), Stoffel & Wielebinski (1978), and Willis & O'Dea (1990). A bridge of emission is seen to connect the bending jet to the outermost component of the north-western lobe, presumably the hot spot (denoted 'A' by Willis et al. 1982).

The steepening of the spectrum is even more pronounced in the south-eastern lobe. In our full-resolution map in Fig. 6a, most of the lobe structure visible at lower frequencies (Waggett et al. 1977; Stoffel & Wielebinski 1978; Jägers 1987; Willis & O'Dea 1990) has decreased below the 2-σ level, except at $\alpha_{50} \approx 16^h50^m27^s$, δ_{50} = 82°27′.7 (feature 'C' of Willis et al. 1982). The source at α_{50} = $16^h46^m42^s$, δ_{50} = 82°39′.4 is rather detached and shows no significant linear polarization, thus corroborating the conclusion by Stoffel & Wielebinski (1978) that it is an unrelated background source. Before we will have CLEANed our map, nothing can be said at this stage about the visibility of the counterjet reported by Perley et al. (1984) at λ2.8 cm.

Our map of linear polarization of NGC 6251 is shown in Fig. 6b. The structure in the immediate vicinity of the central source is caused by spurious instrumental polarization. The jet shows polarization at about the 5%–10% level, certainly the result of beam depolarization in view of its magnetic field structure seen at high resolution, viz. a perpendicular field on the jet axis,

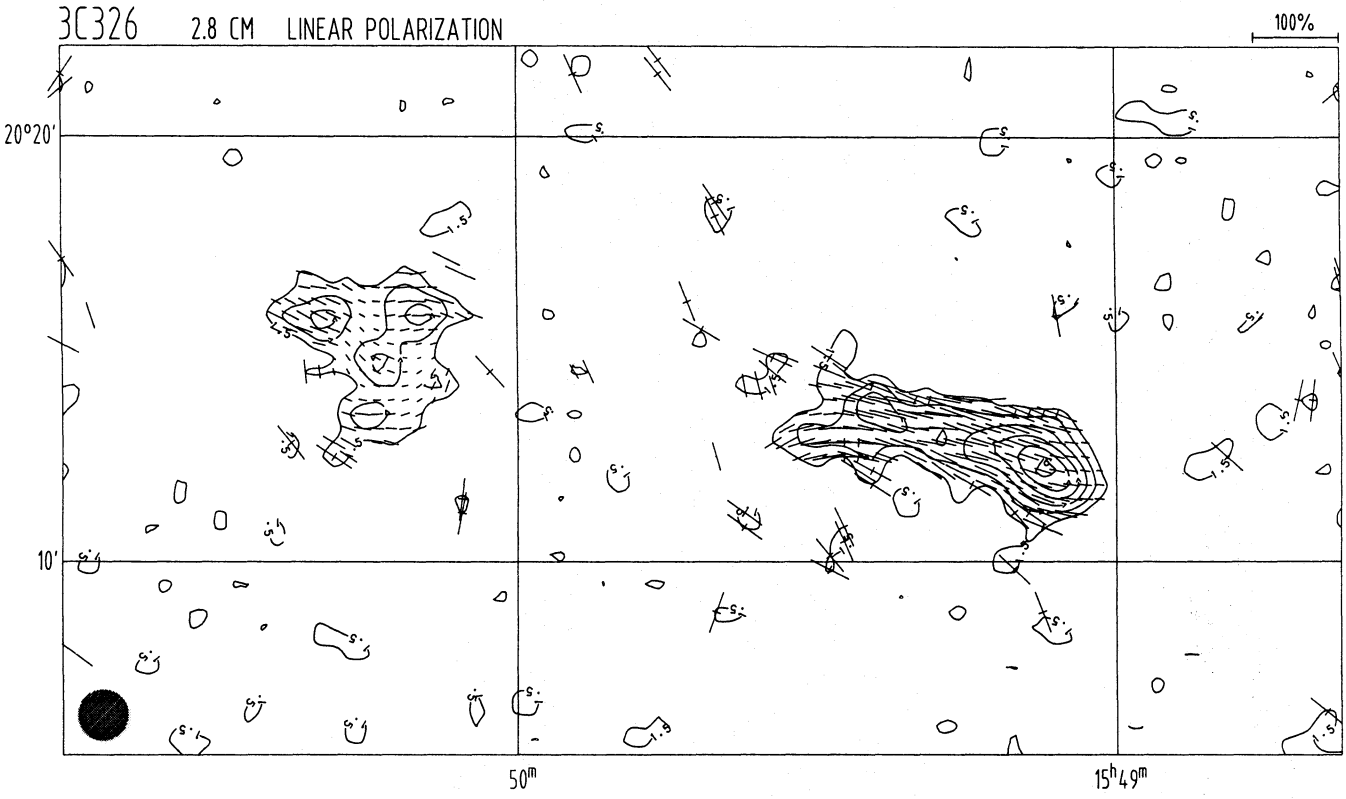

Fig. 5b. Map of the linearly polarized intensity of 3C 326 at λ2.8 cm (same layout as in Fig. 1b)

and a parallel one at its outer edges (Perley et al. 1984). As a result of this beam smearing and depolarization, the mean field orientation visible at λ2.8 cm with our 69″ beam makes an angle of $\sim$ 60° with respect to the jet axis at its brightest part, while further out ($\sim$ 6′ from the core) it is perfectly perpendicular to the jet. This trend appears to maintain throughout the region of the jet bending into the lobe. The hot spot itself is surrounded by a circumferential field, with high degrees ($p_{2.8}$ $\sim$30–40%) of linear polarization marking the outer lobe edges. This does not quite confirm the very high values of fractional polarization reported by Willis et al. (1978), Stoffel & Wielebinski (1978), and Jägers (1979). The south-eastern lobe exhibits high degrees of polarization at feature 'C' of Willis et al. (1982) only, with $p_{2.8} \simeq$30–40%. The magnetic field is essentially perpendicular to the source axis there. Comparison of our $\boldsymbol{B}$-vectors with the $\boldsymbol{E}$-vectors measured at λ11 cm by Stoffel & Wielebinski (1978) suggests the presence of significant Faraday rotation at lower frequencies. This may be caused by the Galactic foreground medium. The density of the (hot thermal) gas surrounding NGC 6251 is certainly low. Recent X-ray observations with ROSAT revealed that the extent of the hot gaseous halo of the host galaxy is only $\lesssim$ 3 kpc (Birkinshaw & Worrall 1993).

4. Summary and discussion

All of the sources discussed here have at least one component which is strikingly broad at low frequencies, and in most cases it holds for both components. At λ2.8 cm, however, the lobes are almost invariably narrower, and sometimes shorter as well. These regions of spectral steepening presumably reflect radiation losses, suggesting that particles diffuse primarily laterally away from the component major axes.

A major exception to this is the entire extended region south of the NW jet/lobe of NGC 315, which looks much like the low-frequency maps. One can speculate that here we are perhaps seeing emission not from a lobe but from cosmic rays which have leaked into the IGM around NGC 315. It may be that the magnetic field in the IGM is lower than that in the components, and since the spectral break frequency varies as $\nu \sim B^{-3} \cdot t^{-2}$, particles in a weaker field radiate longer before suffering noticeable energy losses. However, since they probably diffuse at something like the Alfvén speed ($\sim B \cdot n^{-1/2}$), the particle density in the IGM would also have to be lower if they are to get out fast enough. This would mean a particle energy density above equipartition (to compensate for the low magnetic field strength) which would have consequences for the Inverse Compton emission from the region: NGC 315 would be a good candidate.

Alternatively, the radio arc could be the projected 'fluorescent' trace of the hot spot, 'painted' on the sky by a precessing jet (see e.g. Ekers et al. 1978). The arc appears to delineate a half circle. It is noteworthy that throughout this arc the magnetic field orientation appears to be parallel to the field at the outer edge of the hot spot (Fig. 1c). If the magnetic field structure in the radio arc is a relic of the compressed magnetic field of the hot spot path delineated by the precessing beam, the projected

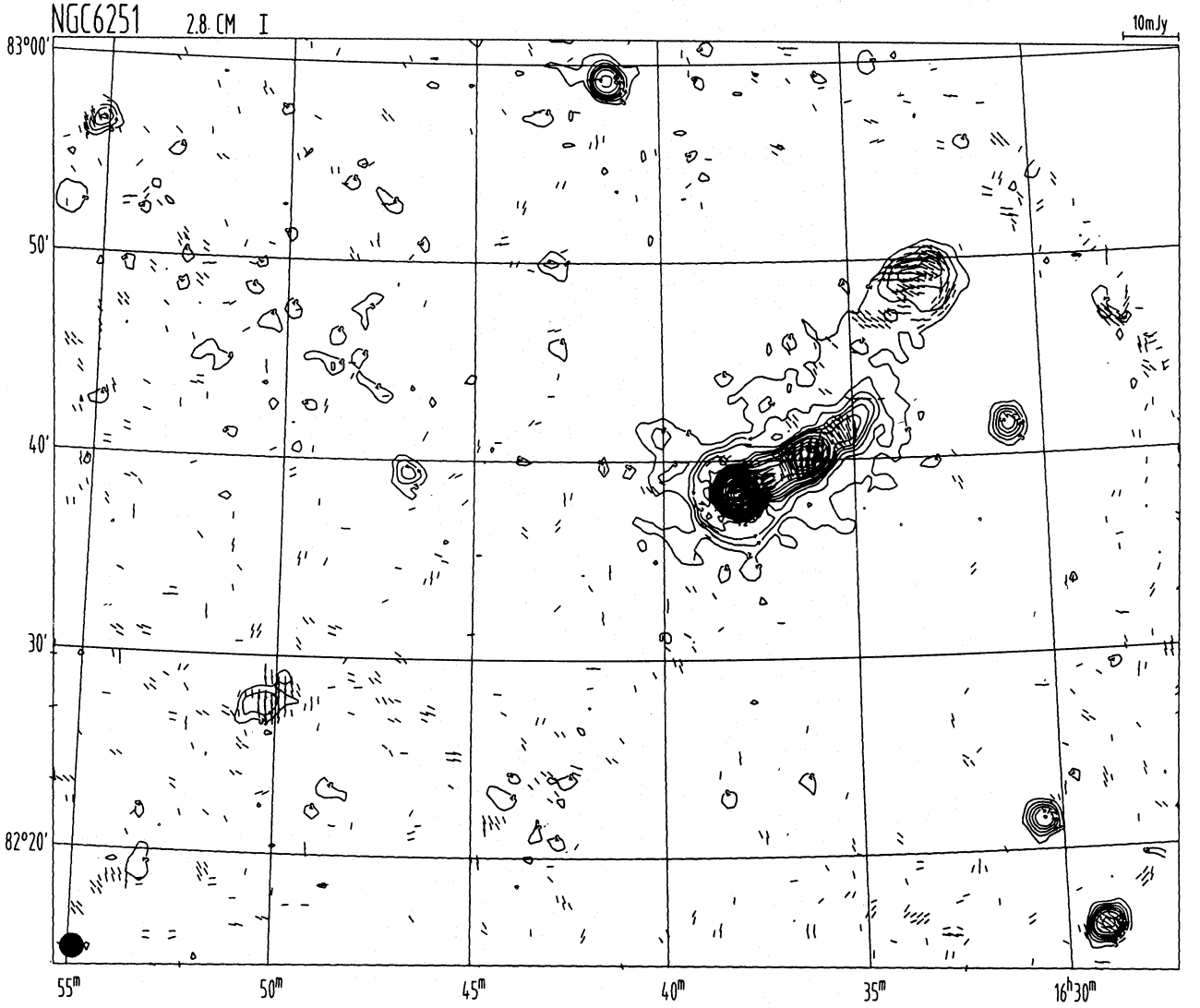

Fig. 6a. Map of the total intensity of NGC 6251 at $\lambda 2.8$ cm (same layout as in Fig. 1a)

orientation of the magnetic field may tell us something about the source orientation. If we would witness the source precessing 'end-on', the $\boldsymbol{B}$-field left behind by the hot spot should show an essentially constant orientation. If the precession happened to be in the plane of the sky, we would expect a concentric orientation around the central source. The fact that the observed situation resembles the former case (Fig. 1c) therefore leads us to conclude that the precession is significantly inclined with respect to the plane of the sky.

Both, leakage as well as precession of the jet, face, however, the problem that the extended arc has a very flat spectrum south of the nucleus of NGC 315. A preliminary comparison with low-frequency data indicates $\alpha \simeq -0.3 \ldots -0.2$ there! With a density of the surrounding IGM of a few $\times 10^{-4}\,\mathrm{cm}^{-3}$ an Alfvénic speed of $\sim 1000 \ldots 2000\,\mathrm{km\,s}^{-1}$ would have to be inferred. The (projected) length of the arc is about 500 kpc, implying a propagation time of $\sim 5 \ldots 10 \cdot 10^8$ yrs for leaking particles. One would expect significant energy losses (synchrotron plus inverse Compton) within this time scale. On the other hand, assuming a break frequency above 10 GHz, a particle age of well below 10^8 yrs results. An equipartition magnetic field strength of a few μG has been inferred from the brightness at $\lambda 2.8$ cm.

Hot spots in the lobes are generally as prominent at $\lambda 2.8$ cm as at long wavelengths. They are thus likely sites of particle acceleration or injection. The nuclear components also have flat spectra, in some cases even inverted at low frequencies, like NGC 315 (Fanti et al. 1986), but this is almost certainly the result of synchrotron self-absorption: the turnover frequency can be used to estimate their angular diameter.

If the components themselves expand laterally, we have one possible explanation that the magnetic field usually runs roughly parallel to contours of total intensity, given that the field is frozen into the plasma. A radially directed field varies as r^{-2}, while a tangentially directed one goes as r^{-1}: the radial field will be expanded out, providing a natural explanation for the dominant tangential fields observed. It may then not be too surprising that we find very high degrees of linear polarization, indicating practically no disordering the magnetic field geometry. These

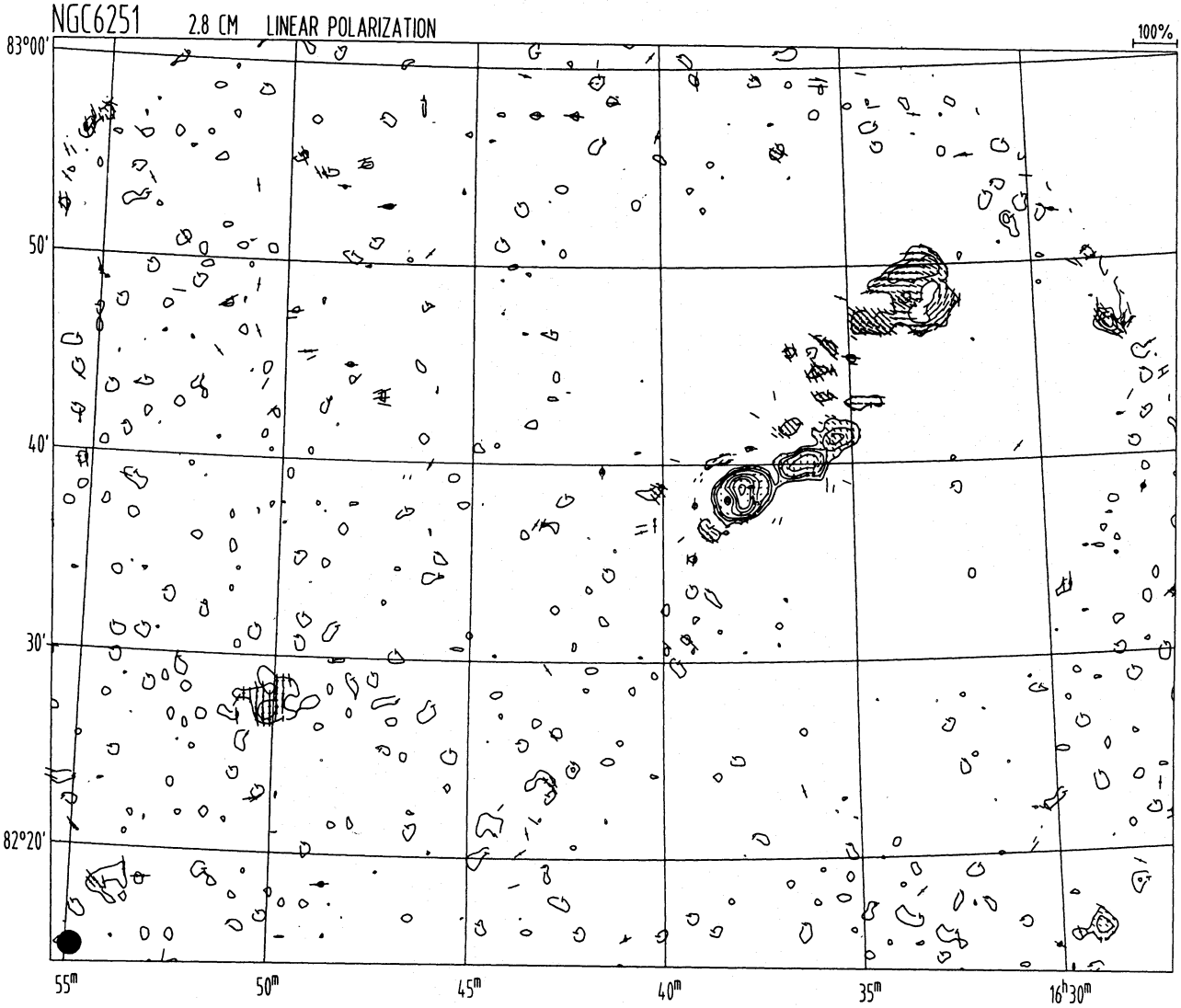

Fig. 6b. Map of the linearly polarized intensity of NGC 6251 at λ2.8 cm (same layout as in Fig. 1b)

are very relaxed components, relatively free of turbulence and irregularities. One exception to this rule appears to be in the eastern component of 3C 326, although its lower degree of linear polarization could be caused by back-to-front interference and need not be the result of small-scale field disorder.

A bending circumferential magnetic field is frequently seen at the outer edges of the hot spots of the GRGs studied here. This is probably the result of compression and alignment caused by the thrust of the jets as they plunge through the IGM.

Finally, we note that both the low rate of depolarization with wavelength and the low rotation measures generally observed indicate low plasma densities within the components. This, too, is consistent with components which have undergone great expansion, as suggested by Strom (1972) on the basis of integrated polarizations of many sources. It is also in line with the small extent of the X-ray corona reported for NGC 6251 by Birkinshaw & Worrall (1993).

Acknowledgements. U.K. is grateful for the hospitality at the Radiosterrenwacht Dwingeloo, where part of the discussions for this paper took place.

References

Baars J.W.M., Genzel R., Pauliny-Toth I.I.K., Witzel A., 1977, A&A 61, 99
Baker J.R., 1974, Mem. Soc. Astron. Ital. 45, 579
Baker J.R., Preuss E., Whiteoak J.B., Zimmermann P., 1974, Nat 252, 552
Barthel R.D., Schilizzi R.T., Miley G.K. et al., 1985, A&A 148, 243
Birkinshaw M., Worrall D.M., 1993, ApJ (submitted)
Bridle A.H., Davis M.M., Fomalont E.B., Lequeux J., 1972, AJ 77, 405
Bridle A.H., Davis M.M., Meloy D.A. et al., 1976, Nat 262, 179
Bridle A.H., Davis M.M., Fomalont E.B. et al., 1979, ApJ 228, L9
Ekers R.D., Fanti R., Lari C., Parma P., 1978, Nat 276, 588
Emerson D.T., Gräve R., 1988, A&A 190, 353
Emerson D.T., Klein U., Haslam C.G.T., 1979, A&A 76, 92

Fanti R., Lari C., Spencer R.E., Warwick R.S., 1976, MNRAS 174, 5P
Fomalont E.B., Bridle A.H., Willis A.G., Perley R.A., 1980, ApJ 237, 418
Gregorini L., Klein U., Parma P. et al., 1992, A&AS 94, 13
Jägers W.J., 1986, Ph.D. thesis, University of Leiden
Jägers W.J., 1987a, A&AS 71, 75
Jägers W.J., 1987b, A&AS 71, 603
Laing R.A., 1980, MNRAS 193, 439
Mack K.-H., Gregorini L., Parma P., Klein U., 1993, A&A (in press)
Mackay C.D., 1969, MNRAS 145, 31
Mayer C.J., 1979, MNRAS 186, 99
Muxlow T.W.B., Garrington S.T., 1991. In: Hughes P.A. (ed.) Beams and Jets in Astrophysics. Cambridge Univ. Press, p. 52
Perley R.A., Bridle A.H., Willis A.G., 1984, ApJS 54, 291
Saunders R., Baldwin J.E., Pooley G.G., Warner P.J., 1981, MNRAS 197, 287
Sofue Y., Reich W., 1979, A&A 38, 251
Stoffel H., 1978, Diploma thesis, University of Bonn
Stoffel H., Wielebinski R., 1978, A&A 68, 307
Strom R.G., 1972, Nat Phys. Sci. 239, 19
Strom R.G., Willis A.G., 1980, A&A 85, 36
Strom R.G., Baker J.R., Willis A.G., 1981, A&A 100, 220
Tsien S.C., 1982, MNRAS 200, 377
Waggett P.C., Warner P.J., Baldwin J.E., 1977, MNRAS 181, 465
Wardle J.F.C., Kronberg P.P., 1974, ApJ 194, 249
Willis A.G., O'Dea C.P., 1990. In: Beck R., Kronberg P.P., Wielebinski R. (eds.) Proc. IAU Symp. 140, Galactic and Intergalactic Magnetic Fields. Kluwer, Dordrecht, p. 455
Willis A.G., Strom R.G., 1978, A&A 62, 375
Willis A.G., Strom R.G., Wilson A.S., 1974, Nat 250, 625
Willis A.G., Wilson A.S., Strom R.G., 1978, A&A 66, L1
Willis A.G., Strom R.G., Bridle A.H., Fomalont E.B., 1981, A&A 95, 250
Willis A.G., Strom R.G., Perley R.A., Bridle A.H., 1982. In: Heeschen D.S., Wade C.M. (eds.) Proc. IAU Symp. 97, Extragalactic Radio Sources. Reidel, Dordrecht, p. 141

This article was processed by the author using Springer-Verlag TEX A&A macro package 1992.